Applied Geochemistry 24 (2009) 1251–1260

Contents lists available at ScienceDirect

Applied Geochemistry

journal homepage: www.elsevier.com/locate/apgeochem

Stability of phyllosilicates in $Ca(OH)_2$ solution: Influence of layer nature, octahedral occupation, presence of tetrahedral Al and degree of crystallinity

M. Mantovani [a], A. Escudero [b], M.D. Alba [a], A.I. Becerro [a,*]

[a] Instituto de Ciencia de Materiales de Sevilla, Departamento de Química Inorgánica (CSIC-US) Avda. Américo Vespucio, s/n. 41092 Sevilla, Spain
[b] Bayerisches Geoinstitut, Universität Bayreuth, Bayeruth 95440, Germany

ARTICLE INFO

Article history:
Received 29 April 2008
Accepted 20 March 2009
Available online 5 April 2009

Editorial handling by M. Gascoyne

ABSTRACT

This paper presents the results of a comprehensive investigation of the interaction of layered silicates with $Ca(OH)_2$ in hydrothermal conditions. The study is intended to evaluate the stability of the clay buffer in radioactive waste repositories, at the intermediate stages of concrete leaching, when the pH is controlled by the dissolution of portlandite. The influence of layer nature, octahedral occupation, presence of tetrahedral Al and degree of crystallinity will be assessed by analysing the behaviour of a set of well-selected phyllosilicates and using the combined capabilities of ^{29}Si and ^{27}Al MAS-NMR spectroscopy, powder X-ray diffraction and SEM/EDX. The results show that the main factor affecting the stability of the clay is the octahedral occupation, so that trioctahedral phyllosilicates are much more stable than dioctahedral ones. The nature and expandability of the layer does not seem to much influence the stability of the clay, so that a 2:1 expandable phyllosilicate shows the same stability as a chemically analogous 1:1 non-expandable phyllosilicate. However other factors like the poor crystallinity of the starting material or the presence of Al in the tetrahedral sheet of trioctahedral phyllosilicates weaken the clay structure in alkaline conditions and favour the transformation towards other phases.

1. Introduction

High pH solution-mineral reactions occur in a variety of geological environments as well as when the environment has been modified by human activity in various engineering projects, such as emplaced concrete. Concrete and cement are proposed as matrix material, backfill material and structural components of radioactive waste repositories (Glasser, 2001). Solidification or disaggregation of concrete will produce high pH solutions. The release of this alkaline, high pH plume to the surrounding media has been modelled (Reardon, 1990; Vieillard and Rassineux, 1992) showing first a period of NaOH and KOH release (pH > 13.5), followed by a solution composition controlled by portlandite ($Ca(OH)_2$) (pH = 12.5) and finally a solution composition controlled by Ca-silicate-hydrate (CSH) gels (pH = 9–10). The effect of such high pH conditions may be of importance for all components in the repository, i.e., the rock fracture minerals where the repository is placed, the bentonite buffer surrounding the canisters where the fuel rods are encapsulated, the canister itself and, finally, the spent fuel in case of failure of the enclosing barriers. The clay buffer is of special concern since moderate mineralogical changes may lead to reduction, and eventually, to loss of the indispensable sealing and mechanical properties of the buffer (Pusch and Yong, 2003; Pusch et al., 2003).

Previous studies on the reactivity of clays in alkaline solutions have been based, mostly, on the behaviour of the layered silicates in KOH and NaOH solutions (short-term initial stage of the concrete leaching). They have focused on the collapse of expandable smectite layers, in particular on the formation of illite/smectite mixed-layers and on the illitization of kaolinite (Huang, 1993; Bauer and Berger, 1998; Bauer et al., 1998; Bentabol et al., 2003). Rassineux et al. (2001) carried out Wyoming interaction tests with a 0.5 M Na–K–Ca alkaline solution, showing minor interlayering effects but the formation of beidellitic smectites. Other authors have reported the alkaline dissolution of montmorillonite and the formation of Na/K-zeolites and trioctahedral Mg smectite (Vigil et al., 2001; Ramírez et al., 2005; Sánchez et al., 2006). Clay alteration at mid-term (pH = 12.5 caused by $Ca(OH)_2$ dissolution) has been less studied and mostly with montmorillonite; it is characterized by the formation of CSH gels and Mg clays in the concrete–clay interface (Read et al., 2001; Savage et al., 2002; Ramírez et al., 2002).

Despite the numerous studies described above, a systematic analysis of the behaviour of different layer structure and composition phyllosilicates with a wide characterization of the obtained solids and a complete discussion of the factors influencing the stability in alkaline solutions is lacking in the literature. For this reason, the target here is to study the behaviour of a set of carefully selected phyllosilicates, submitted to hydrothermal treatment in alkaline conditions at the intermediate stages of concrete leaching, when the pH is controlled by the dissolution of portlandite

* Corresponding author. Fax: +34 954460665.
E-mail address: anieto@icmse.csic.es (A.I. Becerro).

0883-2927/$ - see front matter © 2009 Elsevier Ltd. All rights reserved.
doi:10.1016/j.apgeochem.2009.03.012

($Ca(OH)_2$). Phyllosilicates of different structural nature and chemical composition have been selected in order to study the influence of the following factors on their stability under the described alkaline conditions:

- the octahedral sheet occupation: both tri and dioctahedral phyllosilicates are studied,
- the degree of crystallinity: two kaolinite samples with different crystallinity degrees and two trioctahedral smectites, very similar in composition but with different crystallisation degree have been used,
- the layer structure: 1:1 (kaolinites) and 2:1 (smectites) samples have been selected,
- the presence of Al substituting for Si in the tetrahedral sheet of the clay: two dioctahedral smectites with and without tetrahedral Al (beidellite and montmorillonite, respectively) and two trioctahedral smectites with and without tetrahedral Al (saponite and hectorite, respectively) are studied to assess the influence of this factor on the stability of the clays.

In the course of the experiments, some interesting observations regarding the formation of different $CaSi_2Al_2O_8$ polymorphs were noticed, which are also analysed in detail.

The resultant solids from the hydrothermal reactions have been studied by means of both long- and short-range order techniques. X-ray diffraction patterns have been used to identify any new crystalline phases resulting from the hydrothermal treatments. ^{29}Si MAS NMR (Magic Angle Spinning Nuclear Magnetic Resonance) spectroscopy has been used to observe any Si-containing amorphous phase not detected by diffraction, as well as to quantify the percentage of Si-containing phases. ^{27}Al MAS NMR spectra have been recorded in order to study any diffusion of Al inside the phyllosilicate framework or towards new phases formed as a consequence of the reaction. Finally, Scanning Electron Microscopy with EDX analysis has been used to study aspects of $CaSi_2Al_2O_8$ polymorphism, as commented above.

2. Experimental

2.1. Starting materials

Seven well-characterized phyllosilicates were selected for investigation (structural formulae are shown in Table 1). Two of them are 1:1 phyllosilicates, while the rest have a 2:1 layer structure. The 1:1 phyllosilicates selected are two kaolinites (dioctahedral character and neutral layer charge) with different degrees of crystallinity; KGa-1b is a well-crystallized kaolinite while KGa-2 is poorly crystallized. Among the 2:1 phyllosilicates selected, there are 2 dioctahedral (montmorillonite and beidellite) and 3 trioctahedral (saponite, hectorite and laponite) members. Two of them (beidellite and saponite) contain Al substituting for Si in the tetrahedral sheet of the clay, while the rest exclusively exhibit Si in the tetrahedral sheet. Finally, hectorite and laponite differ in their degree of crystallization, which is poorer in the latter because it is a synthetic sample. All the 2:1 phyllosilicates analysed have a layer charge deficit in the range corresponding to smectites, in agreement with the *Association International pour ÍEtude des Argilles Nomenclature Committee (1980)*. All the silicates, except laponite, are natural samples and were supplied by the Source Clay Minerals Repository, University of Missouri (Columbia). Laponite is a synthetic hectorite and was obtained from Solvay Alkali GMBH. Original samples with particle diameter <2 μm were used, after removal of carbonates and organic matter.

2.2. Hydrothermal treatments

Three-hundred milligrams of the powdered clay and 50 mL $Ca(OH)_2$ solution 0.0223 M (intermediate stage of concrete diasaggregation, Andersson et al., 1989) were transferred into stainless steel T316SS hydrothermal reactors, which were heated to 300 °C for 5 days. The internal pressure corresponds approximately to the water vapour pressure at that temperature (8.58 MPa). At the end of the reaction time, the reactors were cooled to room temperature and the solids were separated by filtration, washed repeatedly with distilled water and allowed to dry in air at 40 °C. Although it is well-known that geochemical processes of waste degradation and waste/rock interaction in the hydrothermal environment remain predictable to temperatures up to about 200 °C, many studies devoted to simulating deep geological disposal conditions use temperatures of up to 350 °C to increase reaction rates (Mather et al., 1982; Savage and Chapman, 1982; Allen and Wood, 1988; Alba and Chain, 2007).

2.3. Characterization techniques

X-ray powder diffraction (XRD) patterns were carried out using a Siemens D-501 diffractometer, with Ni-filtered Cu Kα radiation, steps of 0.05° and counting time of 3 s. ^{29}Si Magic Angle Spinning Nuclear Magnetic Resonance (MAS-NMR) spectroscopy measurements were carried out in a Bruker DRX400 (9.39 T) spectrometer equipped with a multinuclear probe, using 4 mm zirconia rotors spinning at 10 kHz. A single pulse sequence was used, with a pulse length of 2.5 μs (π/2 pulse length = 7.5 μs), an observation frequency for ^{29}Si of 79.49 MHz, and an optimised delay time of 15 s. The chemical shifts are reported in ppm from Tetramethylsilane (TMS). ^{27}Al MAS NMR spectra were recorded at 104.26 MHz with a pulse length of 1.1 μs (π/2 pulse length = 11 μs), a delay time of 0.5 s. The chemical shifts are reported in ppm from a 0.1 M $AlCl_3$ solution. The experimental ^{29}Si NMR spectra of the starting materials and the reaction products have been fitted to the individual contributions of the different phases containing Si that had been previously found in the corresponding XRD patterns. However, following this strategy, one or two regions of some of the spectra remained misfit, due, for example, to the fact that NMR sees both crystalline and amorphous phases, while X-ray diffraction patterns do no account for amorphous phases. Therefore, in addition to the contributions produced by the phases observed in the XRD patterns, low intensity curves have been necessary to obtain a good fit in certain spectra, which have subsequently been assigned to the corresponding environments. A modified version of the Bruker Winfit program which handles the finite spinning speed in MAS experiments (Massiot et al., 2002), has been used for the modelling. Finally, Scanning Electron Microscopy was carried out in a JEOL JSM 5400 microscope equipped with a LINK Pentafet probe and ATW windows for Energy Dispersive X-ray Analysis (EDX).

3. Results

3.1. XRD study

3.1.1. XRD study of the starting materials

The bottom plots of Figs. 1a–d and 2a–c show the X-ray diffraction patterns of the starting materials. In general, the XRD pattern of layered silicates consists of two types of reflections, basal (symmetric lines, 0 0 *l*) and general (asymmetric ones, *hk*). The position of the basal reflections varies, in the case of smectites, with the separation between the layers. The 0 0 1 basal spacing of the non-treated smectites ranges from 12.5 Å in saponite and hectorite to 15.3 Å in montmorillonite, corresponding two different degrees of hydration of the corresponding interlayer cations

Table 1
Structural formula of the studied phyllosilicates.

Sheet	Cations	1:1 Phyllosilicates		2:1 Phyllosilicates				
		Dioctahedral		Dioctahedral		Trioctahedral		
		Kaolinite KGa-1b[a]	Kaolinite KGa-2[a]	Montmorillonite SAz-1[a]	Beidellite SBCa-1[b]	Saponite sapCa-1[c]	Hectorite SHCa-1[c]	Laponite[c]
IV	Si(IV)	3.83	4.00	8.00	7.56	7.20	7.96	8.0
	Al(III)	0.17	–	–	0.44	0.80	0.04	–
VI	Al(III)	3.86	3.66	2.71	3.63	–	0.04	–
	Mg(II)	–	tr	1.11	0.19	5.79	5.30	5.45
	Li(I)	–	–	–	–	–	0.66	0.40
	Fe(III)	0.02	0.07	0.12	0.18	0.14	–	–
	Mn(II)	tr	tr	0.01	–	–	–	–
	Ti(IV)	0.11	0.16	0.03	–	–	–	–
Interlayer	Ca(II)	0.01	tr	0.39	0.63	0.09	0.33	–
	Na(I)	0.01	–	0.29		0.61	–	0.70
	K(I)	0.01	tr	0.02		0.02	–	–
	Mg(II)	0.02	–	–	–	–	–	–

Kaolinite KGa-1b: is a well-crystallised kaolinite.
Kaolinite KGa-2: is a poorly-crystallised kaolinite.
Structural formula taken from:
[a] Clay source repository web page.
[b] Becerro (1997).
[c] Chain (2007).

(see Table 1). The poor crystallinity of the synthetic laponite (Fig. 2c, bottom) hinders calculation of the basal spacing due to the lack of resolution in the 0 0 l reflections. Both kaolinite samples show the basal spacing typical of this layer silicate (7.1 Å), much lower than that observed in the smectite samples due to the absence of both one tetrahedral sheet per layer and interlayer cations. The general nature of the *hk* band system is the same for all the smectites, the differences being in the details of spacing and relative intensities. In particular, spacing values for the 0 6 0 reflection (one sixth of the *b* unit cell parameter) of 1.530 Å and 1.490 Å are characteristic of the trioctahedral and dioctahedral end-members phyllosilicates, respectively (Grim, 1968). The XRD pattern of the non-treated montmorillonite shows a 0 6 0 spacing value of 1.498 Å, a value slightly higher than that in pure dioctahedral phyllosilicates, due to the substitution of Mg^{2+} for Al^{3+} in the octahedral sheet (Desprairies, 1983) (Table 1). The 0 6 0 spacing value in beidellite is 1.491 Å, in agreement with the lower Mg content of the octahedral sheet in comparison with montmorillonite. Saponite shows a 0 6 0 spacing value of 1.527 Å, very close to the value of 1.530 Å for pure trioctahedral samples. However, the values in laponite and hectorite are slightly lower (1.520 Å and 1.511 Å, respectively), due to the partial substitution of Li^{+} by Mg^{2+} in the octahedral sheet. Finally, the 0 6 0 spacing value is 1.49 Å in both kaolinite samples, in good agreement with the pure dioctahedral nature of both kaolinites.

The next section discusses the XRD patterns of the dioctahedral and trioctahedral phyllosilicates after the hydrothermal treatment in $Ca(OH)_2$ solution.

3.1.2. XRD study of the dioctahedral phyllosilicates

The XRD pattern of the montmorillonite after treatment (Fig. 1a, top) shows, in addition to the reflections of montmorillonite, slight changes as otlined below, a set of well resolved reflections indicative of the formation of new crystalline phases, the main ones being the low symmetry triclinic polymorph of anorthite $CaAl_2Si_2O_8$ (PDF 41-1486) and xonotlite ($Ca_6Si_6O_{17}(OH)_2$, PDF 23-0125), a Ca silicate hydrate. A low intensity reflection at 7.8° 2θ indicates the formation of tobermorite 11 Å ($Ca_5(OH)_2Si_6O_{16}{\cdot}4H_2O$, PDF 45-1480) as a minor phase. The basal spacing of montmorillonite decreases very slightly to 14.8 Å, but the remnant clay is clearly expandable. The *b* unit cell parameter cannot be evaluated due to the superposition of anorthite lines on top of the 0 6 0 reflection.

The hydrothermal treatment of beidellite causes the growth of several crystalline phases, the main one being the hexagonal polymorph of $CaAl_2Si_2O_8$ (PDF 31-248), marked with H in the plot (Fig. 1b, top). The reflection at 7.8° 2θ indicates the formation of tobermorite 11 Å and some wollastonite ($CaSiO_3$) reflections can also be observed in the 25–35° 2θ region of the pattern. Some expanded clay is still present after the treatment as inferred by the low intensity 0 0 1 reflection at ca. 6.4° 2θ together with a slightly higher 0 0 3 reflection at ca. 17.9° 2θ, which correspond to a basal spacing of 14.8 Å.

The hydrothermal treatment of the well-crystallised kaolinite sample (Fig. 1c, top) causes the growth of hexagonal $CaAl_2Si_2O_8$ (PDF 31-248) as the main crystalline phase and xonotlite. Reflections of kaolinite are also present in the pattern of the treated sample. The XRD pattern of the poorly-crystallised kaolinite sample (Fig. 1d, top) is very similar to that of the well-crystallised kaolinite, producing hexagonal $CaAl_2Si_2O_8$ as the main crystalline phase after the hydrothermal treatment, with some xonotlite and unchanged kaolinite reflections.

3.1.3. XRD study of the trioctahedral phyllosilicates

The hydrothermal treatment of the three trioctahedral smectites (Fig. 2a–c, top plots) provokes very similar changes in the three samples with xonotlite as the main new phase in the reaction product accompanied by antigorite ($Mg_3Si_2O_5(OH)_4$; PDF 44-1447), more abundant in the saponite sample. Both, basal and structural smectite reflections can be observed in the three patterns, which indicate the permanence of a portion of each phyllosilicate after the treatment. The 0 0 1 reflection in saponite and hectorite shifts towards lower angles ($d_{0\,0\,1} \sim 14.5$ Å), indicating a change in both, type and hydration of the interlayer cations as a consequence of the hydrothermal treatment in $Ca(OH)_2$. A $d_{0\,0\,1}$ spacing value cannot be calculated for laponite due to the very broad nature and lack of definition of the 0 0 l reflections.

The superposition of peaks of different phases as well as the preferred orientation effects of the 0 0 l phyllosilicate planes, make a quantitative analysis of phases from the XRD patterns complicated. In order to overcome this problem, as well as to study the short-range order around the Si atoms, single pulse ^{29}Si MAS NMR spectra have been obtained for all the reaction products. The non-quadrupolar nature of this nucleus makes it feasible to quantify the different Si environments from the integrated area of the corresponding contributions obtained from the deconvolution

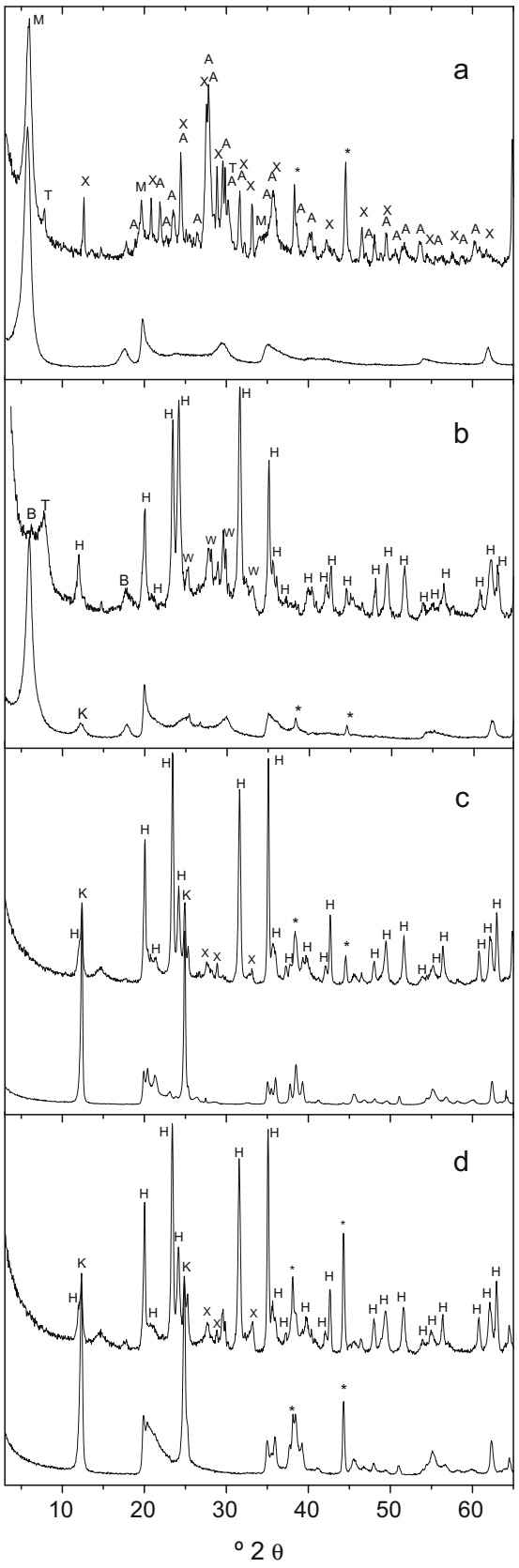

Fig. 1. XRD patterns of the dioctahedral phyllosilicates before (bottom plots) and after (top plots) the hydrothermal treatment in $Ca(OH)_2$ solution. a: Montmorillonite, b: Beidellite, c: well-crystallised kaolinite, and d: poorly-crystallised kaolinite. Reflexions marked with M: Montmorillonite, B: Beidellite, K: kaolinite, T: Tobermorite, X: Xonotlite, A: Triclinic Anorthite, H: Hexagonal $CaAlSiO_8$, and W: Wollastonite, * = Al from the sample holder.

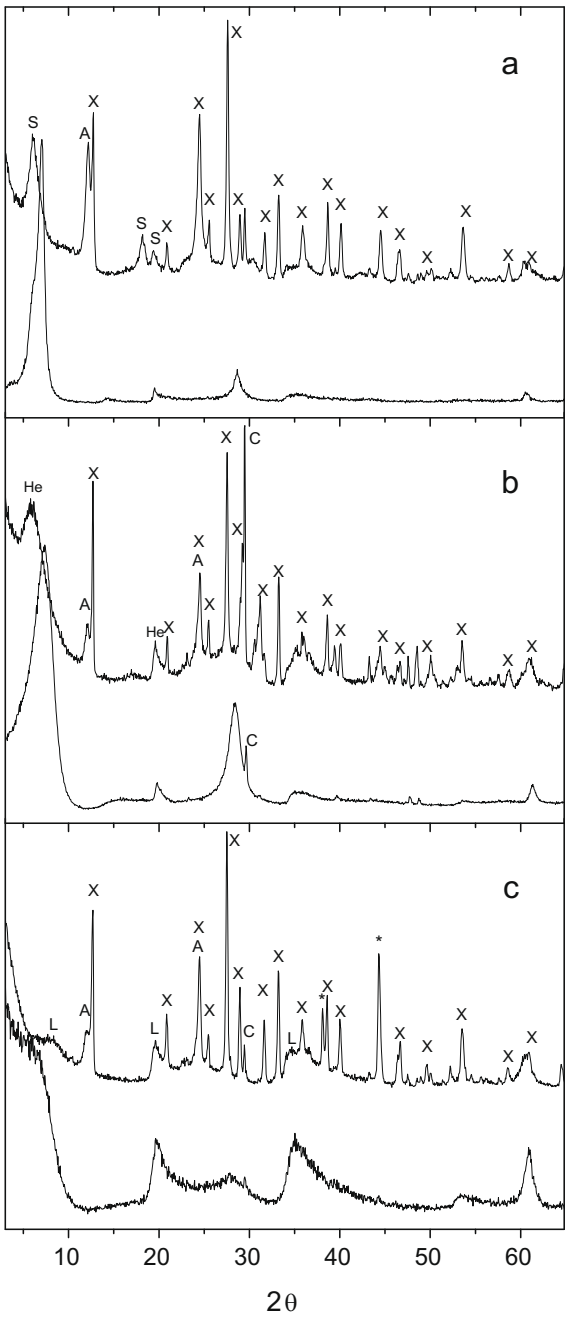

Fig. 2. XRD patterns of the trioctahedral phyllosilicates before (bottom plots) and after (top plots) the hydrothermal treatment in $Ca(OH)_2$ solution. a: Saponite, b: Hectorite, and c: Laponite. Reflexions marked with S: Saponite, He: Hectorite, L: Laponite, A: Antigorite, X: Xonotlite, and C: Calcite, * = Al from the sample holder.

of the experimental spectra. ^{27}Al MAS NMR spectra have also been recorded in the Al-containing clays (montmorillonite, beidellite, both kaolinites and saponite) in order to study the effect of the treatments on the Al environments as well as to observe any diffusion event in the silicate framework as a consequence of the reaction.

3.2. ^{29}Si and ^{27}Al MAS NMR study

3.2.1. ^{29}Si and ^{27}Al MAS NMR study of the starting materials

^{29}Si MAS NMR signals for the starting phyllosilicates (bottom plots of Figs. 3a–d and 4a–c) are in good agreement with those expected for the phyllosilicates with the unit formulae described in

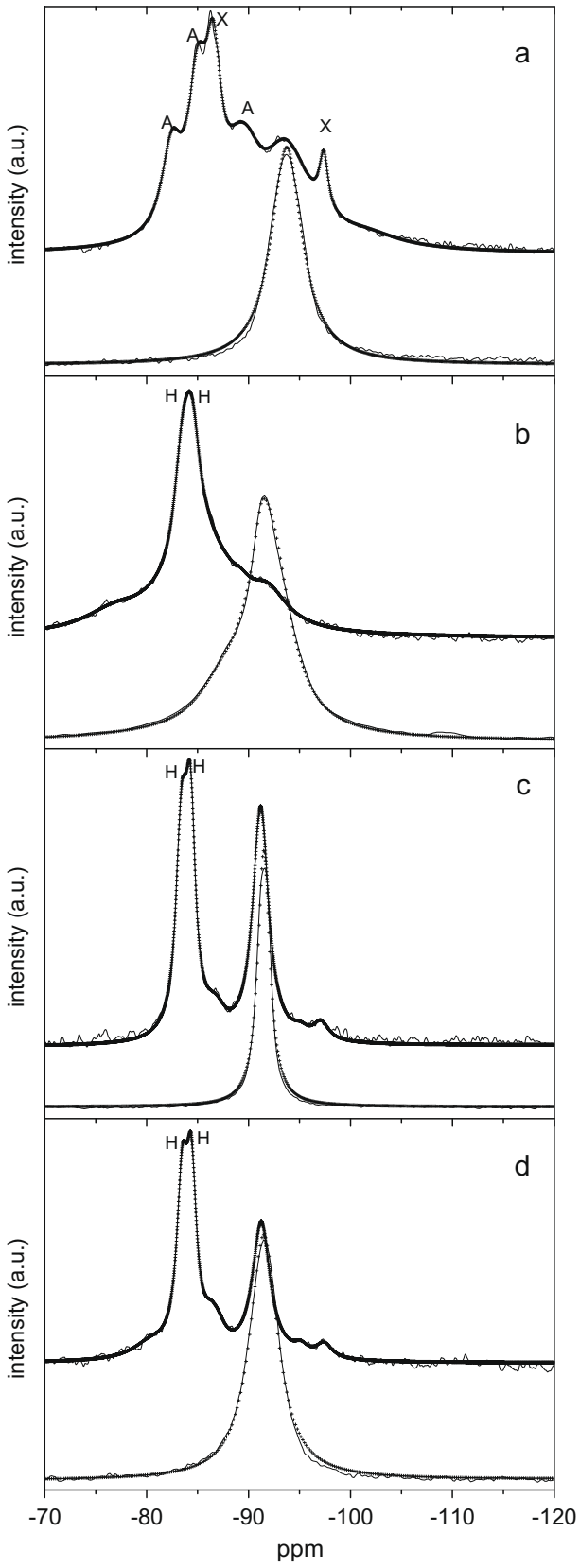

Fig. 3. ^{29}Si MAS NMR spectra of the dioctahedral phyllosilicates before (bottom plots) and after (top plots) the hydrothermal treatment in $Ca(OH)_2$ solution. a: Montmorillonite, b: Beidellite, c: well-crystallised kaolinite, and d: poorly-crystallised kaolinite. Solid line: experimental spectrum. Crosses: Simulated spectrum. Signals marked with X: Xonotlite, A: Triclinic Anorthite ($CaAlSiO_8$), and H: Hexagonal $CaAlSiO_8$.

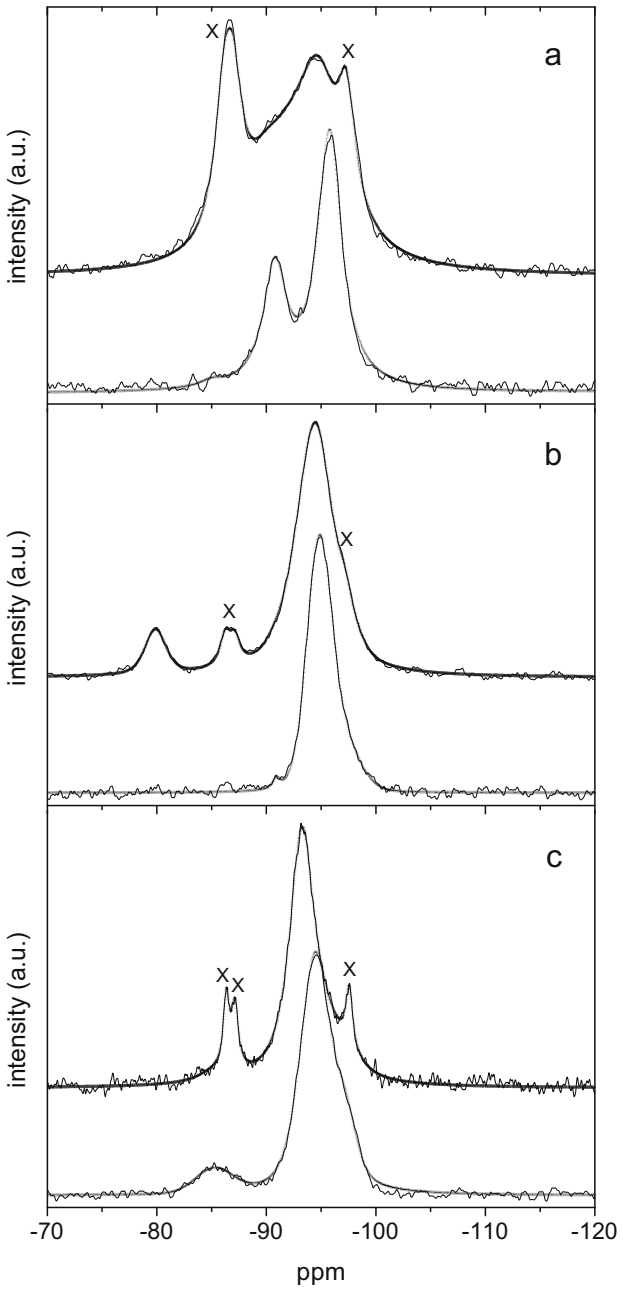

Fig. 4. ^{29}Si MAS NMR spectra of the trioctahedral phyllosilicates before (bottom plots) and after (top plots) the hydrothermal treatment in $Ca(OH)_2$ solution. a: Saponite, b: Hectorite, and c: Laponite. Solid line: experimental spectrum. Crosses: Simulated spectrum. Signals marked with X: Xonotlite.

Table 1. The major component for all the samples corresponds to $Q^3(0Al)$ environments (nomenclature from Liebau, 1985), the differences observed in their chemical shifts being a consequence of both their layer charge values and their octahedral nature (Sanz and Serratosa, 1984). This main signal is the only one that appears in the montmorillonite, and both kaolinite spectra because of the absence or very low content of tetrahedral Al in their structure. The tetrahedral Al content of saponite and beidellite causes additional Si signals at higher frequency values corresponding to $Q^3(1Al)$ and $Q^3(2Al)$ Si environments. Hectorite and laponite, show additional signals due to partially condensed Si tetrahedra, with anionic and hydroxilic basal oxygens (Wheeler et al., 2005). Finally, it is to be noted that the unique ^{29}Si resonance of the starting poorly-crystallised kaolinite (Fig. 3d, bottom) shows a FWHM va-

lue much higher than that of the well-crystallised kaolinite (Fig. 3c, bottom), corresponding to the higher degree of disorder around the Si atoms in the poorly crystallised sample. The same difference in FWHM is observed between hectorite and laponite. The integrated intensities of these contributions, calculated from theoretical Lorentzian curves, are included in Tables 2–4 and are in good agreement with the $^{[IV]}$Al/Si ratios shown in their structural formulae.

The ^{27}Al MAS NMR spectra of the Al-containing starting clays are shown in the bottom plots of Fig. 5a–e. The spectra of the dioctahedral samples (montmorillonite, beidellite and both kaolinites) consist of a signal at ca. 0 ppm corresponding to octahedral Al, while saponite shows a resonance at ca. 65 ppm assigned to tetrahedral Al (Sanz and Serratosa, 1984). This signal is also observed in the beidellite spectrum due to the presence of Al substituting for Si in the tetrahedral sheet of this clay (see Table 1). The low intensity resonance observed at ca. 56 ppm in the montmorillonite spectrum should be assigned to tetrahedral Al not belonging to the clay but to a feldspar impurity, in accordance with the data reported by Kirkpatrick et al. (1985). Finally, the asymmetry presented by the octahedral Al band in the montmorillonite spectrum has been assigned by Woessner (1989) to the existence of several sites of ^{27}Al with the same coordination and similar chemical shift (δ) values but different quadrupolar coupling constants (QCC) and asymmetry parameter (η) values.

3.2.2. ^{29}Si and ^{27}Al MAS NMR study of the treated dioctahedral samples

Up to 6 different resonances can be distinguished in the profile of the ^{29}Si MAS NMR spectrum of montmorillonite after the hydrothermal treatment (Fig. 3a, top), indicating the great variability of Si environments created as a consequence of the reaction, com-

Table 2
^{29}Si chemical shift, FWHM and area under the curve of the different contributions obtained from the fitting of the ^{29}Si MAS NMR spectrum of the dioctahedral 2:1 phyllosilicates.

Phase	^{29}Si chemical shift (ppm)	FWHM (Hz)	Integral
Starting montmorillonite			
Q3(0Al)	−93.7	294	100
Treated montmorillonite			
Montmorillonite			
Q^3(0A1)	−93.7	463	31
Q^3(1A1)	−88.8	270	15
Xonotlite	−97.4	83	3
	−86.3	144	7
	−87.0	145	4
Anorthite (−85 ppm includes	−82.5	190	12
tobermorite)	−85.0	181	18
	−90.1	229	5
Amorphous	−101.6	632	5
Starting beidellite			
Beidellite			
Q^3(0A1)	−91.9	385	82
Q^3(1A1)	−87.2	356	15
Q^3(2A1)	−83.2	190	1
Kaolinite	−91.3	85	2
Treated beidellite			
Beidellite			
Q^3(0A1)	−91.9	369	13
Q^3(1A1)	−86.4	493	24
Q^3(2A1)	−81.1	477	6
Hexagonal $CaSi_2Al_2O_8$	−84.4	162	20
	−83.5	162	16
Wollastonite	−89.2	169	2
	−87.9	154	1
Tobermorite	−85.5	350	7
Amorphous (Na_2SiO_3)	−76.8	581	11

Table 3
^{29}Si chemical shift, FWHM and area under the curve of the different contributions obtained from the fitting of the ^{29}Si MAS NMR spectrum of the dioctahedral 1:1 phyllosilicates.

Phase	^{29}Si chemical shift (ppm)	FWHM (Hz)	Integral
Starting KGa-1b kaolinite			
Q^3(0A1)	−91.5	114	100
Treated KGa-1b kaolinite			
Kaolinite Q^3(0A1)	−91.2	149	43
Hexagonal $CaSi_2Al_2O_8$	−84.3	98	25
	−83.4	104	24
Xonotlite	−97.1	143	3
	−87.1	143	2
	−86.4	143	2
Amorphous	−95.1	137	1
Starting KGa-2 kaolinite			
Q^3(0A1)	−91.5	267	100
Treated KGa-2 kaolinite			
Kaolinite Q^3(0Al)	−91.3	98	33
Hexagonal $CaSi_2Al_2O_8$	−84.4	96	23
	−83.5	102	23
Xonotlite	−97.4	151	4
	−87.0	151	4
	−86.3	155	4
Amorphous	−80.4	343	7
Amorphous	−95.1	131	2

Table 4
^{29}Si chemical shift, FWHM and area under the curve of the different contributions obtained from the fitting of the ^{29}Si MAS NMR spectrum of the trioctahedral 2:1 phyllosilicates.

Phase	^{29}Si chemical shift	FWHM	Integral
Starting saponite			
Saponite			
Q^3(0A1)	−95.8	211	68
Q^3(1A1)	−90.8	204	30
Q^3(2A1)	−85.0	199	2
Treated saponite			
Saponite			
Q^3(0A1)	−95.1	287	23
Q^3(1A1)	−89.7	356	14
Q^3(2A1)	−85.0	278	4
Xonotlite	−97.4	167	10
	−87.0	167	12
	−86.2	167	13
Antigorite	−92.7	357	24
Starting hectorite			
Hectorite Q^3(0A1)	−94.8	215	85
Si–O without H^+	−96.9	281	15
Treated hectorite			
Hectorite Q^3(0A1)	−94.5	328	80
Xonotlite	−97.0	103	3
	−87.1	91	3
	−86.3	91	3
Amorphous (sphene)	−79.9	156	8
Antigorite	−93.1	278	3
Starting laponite			
Laponite			
Q^3(0A1)	−94.5	263	79
Si–O (without H^+)	−97.3	188	13
Si–O (with H^+)	−85.2	316	8
Treated laponite			
Laponite			
Q^3(0A1)	−93.3	212	58
Si–O (without H^+)	−95.5	324	17
Si–O (with H^+)	−85.2	278	3
Xonotlite	−97.6	63	6
	−87.1	61	5
	−86.3	52	5
Antigorite	−93.1	238	6

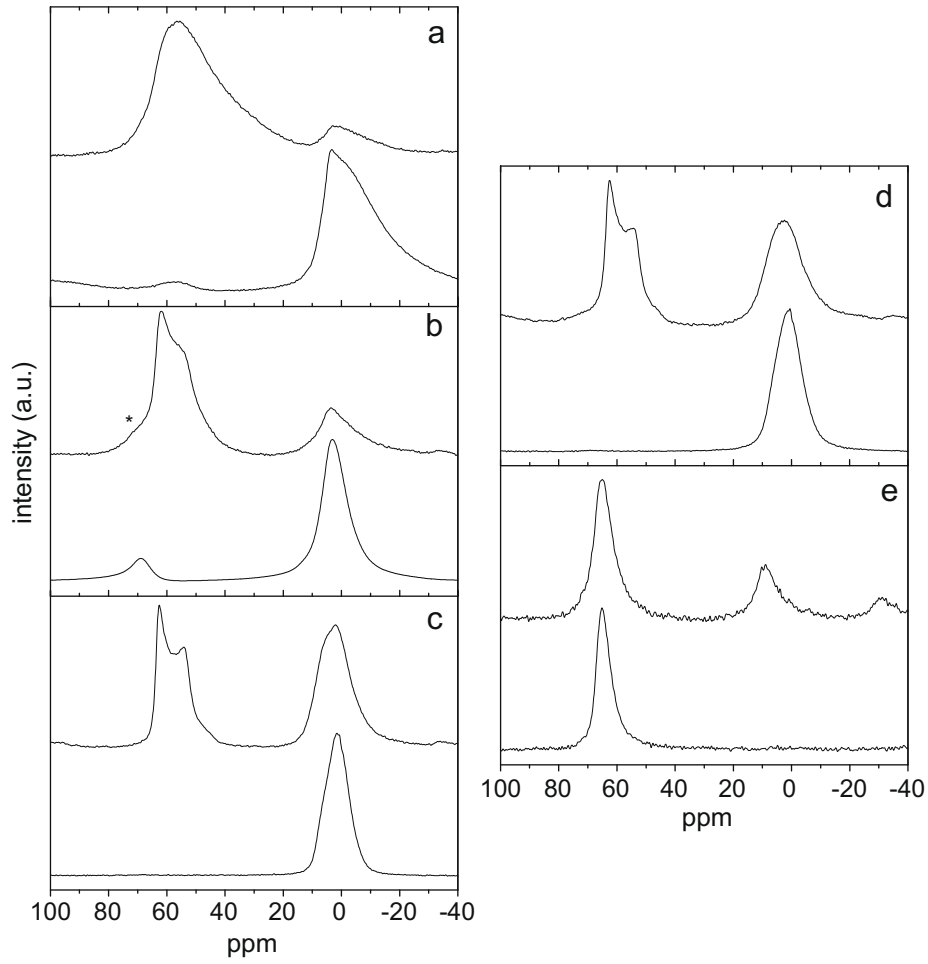

Fig. 5. ^{27}Al MAS NMR spectra of the phyllosilicates before (bottom plots) and after (top plots) hydrothermal treatment in $Ca(OH)_2$ solution. a: Montmorillonite, b: Beidellite, c: well-crystallised Kaolinite, d: poorly-crystallised kaolinite, and e: Saponite, * = Spinning side band.

pared to the unique Si environment in the starting material (Fig. 3a, bottom). The XRD data shows the formation of three different crystalline phases: triclinic anorthite, xonotlite and tobermorite 11 Å. The ^{29}Si chemical shift values for pure triclinic anorthithe (Kirkpatrick et al., 1985), xonotlite (Noma et al., 1998) and tobermorite (Cong and Kirkpatrick, 1996), as described in the literature, are given in Table 5. All those resonances, together with that of montmorillonite have been used as starting parameters for the fitting of the ^{29}Si MAS NMR spectrum of the treated sample. However, the fitting required the use of two additional contributions, as observed in Table 2, at chemical shift values of −88.8 ppm, compatible with Q^3(1Al) environments in the remaining clay, and −101.6 ppm, which can be assigned to an amorphous Si-containing phase not detectable by diffraction. It is also of note that the fitting process did not allow for inclusion of the contribution of tobermorite, due to its proximity to one of the anorthite resonances. Therefore, the area under the resonance curve at −85.0 ppm contains two contributions: one from anorthite and one from tobermorite. The area under the curve values obtained from the fitting of the spectrum indicate that:

(i) almost half of the Si atoms in the sample (46%) are Q^3 environments in the remnant clay,
(ii) thirty-three percent of the Si environments in the clay are surrounded by Al ions, which might indicate diffusion of Al from the octahedral to the tetrahedral sheet of the phyllosilicate as a consequence of the hydrothermal treatment. The ^{27}Al MAS NMR spectrum of the sample should clearly show the partial change in Al coordination from VI to IV. Fig. 5a shows that, while the starting montmorillonite shows almost exclusively an Al resonance at ca. 0 ppm corresponding to octahedral Al, the spectrum of the treated sample shows, in addition, a high intensity broad signal in the chemical shift range typical of tetrahedral Al. However, given that the anorthite structure has Al in tetrahedral sites, the signal observed in the Al spectrum could contain the resonances of Al in both, the anorthite structure and the tetrahedral sheet of montmorillonite,
(iii) thirty-five percent of the Si atoms in the sample are forming part of anorthite and tobermorite while ∼14% are in xonotlite.

The ^{29}Si MAS NMR spectrum of beidellite after the hydrothermal treatment (Fig. 3b, top) is dominated by a main signal centred

Table 5
^{29}Si chemical shift values for the pure minerals, as described in the references given in the text.

Mineral name	^{29}Si chemical shift values (ppm)
Triclinic $CaSi_2Al_2O_8$ (anorthite)	−82.9; −84.8; −89.6
Xonotlite	−97.5; −86.3;−87.1
Tobermorite	−85,3
Hexagonal $CaSi_2Al_2O_8$	−83.0; −84.0
Wollastonite	−87.8; −89.0; −89.5

at ca. −84 ppm and a long tail towards lower frequencies. The XRD pattern showed the formation of hexagonal $CaSi_2Al_2O_8$ as the main phase, together with lower intensity reflections of β-wollastonite and tobermorite 11 Å. The ^{29}Si chemical shift values for pure hexagonal $CaSi_2Al_2O_8$ (Hong et al., 1999), β-wollastonite (Hansen et al., 2003) and tobermorite (Cong and Kirkpatrick, 1996) phases, are given in Table 5. The results of the fitting of the experimental spectrum of the treated beidellite, using the chemical shift values reported for the single phases as starting parameters, is shown in Table 2. As in montmorillonite, an additional contribution, in this case at −76.8 ppm, was necessary to obtain a good fitting, which must correspond to an amorphous Si-containing phase (Na_2SiO_3 gives a resonance at exactly that value, Carpentier et al., 2004). In view of these results, the following observations can be made:

(i) Although the XRD pattern of the sample showed very low intensity reflections corresponding to beidellite, the deconvolution of the ^{29}Si MAS NMR spectrum indicates that ca. 43% of the Si environments in the sample belong to the remnant clay. This fact, together with the high FWHM value of the beidellite Si resonances, indicates a high degree of disorder in the remnant clay.
(ii) Most of the SiO_4 tetrahedra in the clay have some AlO_4 neighbours (∼56% of the total Si environments in the remaining clay are $Q^3(1Al)$ and ∼14% are $Q^3(2Al)$) which implies a massive diffusion of Al from the octahedral to the tetrahedral sheet of the clay. This fact is compatible with the ^{27}Al MAS NMR spectrum of the treated sample (Fig. 5b, top), which shows a main double signal corresponding to Al in hexagonal $CaSi_2Al_2O_8$ (Hong et al., 1999) and a wide shoulder (marked with asterisk) in a frequency region compatible with Al in the tetrahedral sheet of the clay. A considerable decrease in the intensity of the octahedral Al signal is also observed if compared to the same signal in the spectrum of the starting sample (Fig. 5b, bottom).
(iii) ca. 36% of the Si environments in the sample correspond to hexagonal $CaSi_2Al_2O_8$.
(iv) Finally, the area under the curve of the ^{29}Si signal corresponding to Tobermorite, at −85.3 ppm, is 7% while ca. 3% of the Si environments in the sample belong to wollastonite. The high FWHM value obtained for the Na_2SiO_3 contribution indicates the amorphous character of the phase, not visible in the XRD pattern.

Fig. 3c shows the experimental and fitted ^{29}Si MAS NMR spectra of the well-crystallised kaolinite sample before and after the hydrothermal treatment. In good agreement with the XRD pattern of the sample, the ^{29}Si NMR spectrum of the reaction product contains a main double resonance corresponding to Si in hexagonal $CaSi_2Al_2O_8$, and a peak at −91.2 ppm caused by the $Q^3(0Al)$ environments in the remaining kaolinite. The deconvolution of the spectrum (Table 3), however, requires the use of three additional low intensity contributions; two of them, at −86.4 and −97.1 ppm, clearly correspond to xonotlite, which can be recognised after a detailed examination of the XRD pattern. The third is a very low intensity signal at ca. −95.1 ppm which must be produced by an amorphous Si-containing phase. The areas under the individual Si contributions indicate that ca. 43% of the Si environments in the sample correspond to kaolinite, while ∼49% have been transformed into hexagonal $CaSi_2Al_2O_8$. The rest is Si in xonotlite and in the amorphous phase. The ^{27}Al MAS NMR spectrum of the reaction product (Fig. 5c, top) is simple and contains a main double signal corresponding to tetrahedral Al in hexagonal $CaSi_2Al_2O_8$ (Hong et al., 1999) as well as a signal of octahedral Al in the remaining clay. No signs of Al diffusion from the octahedral to the tetrahedral sheet are observed in this case, as opposed to what was observed in montmorillonite and beidellite.

The ^{29}Si MAS NMR spectrum of the poorly-crystallised kaolinite submitted to the hydrothermal treatment (Fig. 3d, top) is very similar to that of the treated well-crystallised kaolinite, with a slightly higher intensity of the hexagonal anorthite double signal compared to the kaolinite signal. The areas under the individual Si contributions (Table 3) indicate that in this case, only 33% of the Si environments in the sample correspond to kaolinite, while ∼46% have been transformed into hexagonal $CaSi_2Al_2O_8$. The rest is Si in xonotlite (∼12%) and in two other Si-containing phases (9%), not detected by XRD analysis, which show signals at −80.4 ppm and −95.1 ppm. The ^{27}Al MAS NMR spectrum of the reaction product (Fig. 5d, top) is very similar to that of treated well-crystallised kaolinite, with a double signal corresponding to tetrahedral Al in hexagonal $CaSi_2Al_2O_8$ (Hong et al., 1999) and a signal of octahedral Al in the remaining clay.

Finally, it is noted that, in all cases, the Si signals corresponding to the clays shift towards higher frequency values after the treatment. Following Sanz and Serratosa (1984) there are three factors that influence the position of the tetrahedral Si signal in phyllosilicates, namely, nature of tetrahedral cations, composition of the octahedral sheet and nature of the interlayer cations. The latter is important when the interlayer cations are dehydrated, as in the case of micas and illites, so that they themselves are the second neighbours of the Si atoms. In the case of the dioctahedral phyllosilicates studied in the present investigation, the shift of the signal towards higher frequencies must be interpreted as being due to the decrease in the occupation of the octahedral sheet as a consequence of the diffusion of Al ions towards the new phases or the tetrahedral sheet of the remnant clay. On the other hand, it can be observed in Tables 2–4, that the contributions corresponding to Si atoms in the remnant clays display higher FWHM values in the treated samples as compared with the starting materials. This fact is interpreted as an increase in the local disorder around the Si atoms after the alkaline reaction.

3.2.3. *^{29}Si and ^{27}Al MAS NMR study of the trioctahedral phyllosilicates*

The ^{29}Si MAS NMR spectrum of saponite after the hydrothermal treatment (Fig. 4a, top) shows three emerging resonances from a broad band that must correspond to Si in xonotlite (Noma et al., 1998) and in the remaining saponite, in agreement with the XRD data. The lack of resolution of the two main saponite resonances, which were clearly observed in the spectrum of the starting saponite (Fig. 4a, bottom) must be due to the presence of the Si signal corresponding to antigorite (at −93.1 ppm in the pure mineral, Kosuge et al., 1995). The deconvolution of the experimental spectrum (Table 4) shows that ∼55% of the Si environments in the sample correspond to saponite, while ∼34% and ∼11% belong to xonotlite and antigorite, respectively. Likewise, the results of the deconvolution show that the percentage of $Q^3(1Al)$ and $Q^3(2Al)$ environments in the remaining saponite has decreased, from 32% to 27%, indicating that the new Si-containing phases form, preferentially, from Si atoms with Al neighbours. This is confirmed by the ^{27}Al MAS NMR spectrum of the sample (Fig. 5e, top) which shows a main signal corresponding to tetrahedral Al at the same position as in the starting clay (Fig. 5e, bottom), but with a higher FWHM value likely caused by the disorder around the remaining Al, once the neighbour Si atoms have left the framework to form new phases. In addition, a lower intensity signal typical of Al in octahedral coordination can be observed in the spectrum of the treated saponite, which could be partially substituting for Mg in the antigorite octahedral sheet.

The ^{29}Si MAS NMR spectrum of the treated hectorite (Fig. 4b, top) displays, in addition to the main signal which corresponds to Si in the remaining hectorite, two new contributions on the high

frequency side. The band centred at ca. −86 ppm must contain two Q^2 signals of xonotlite, while the Q^3 signal of this phase is observed as a shoulder on the low frequency side of the main signal (Noma et al., 1998). The resonance at −79.9 ppm indicates the presence of incipient nuclei of an amorphous phase with Si, possibly in Q^0 environments, and not detected by diffraction; a chemical shift value of −80 ppm has been reported for sphene, an orthosilicate made up of Ca, Si, Ti and O (Sheriff et al., 1991). The deconvolution of the experimental spectrum (Table 4) indicates that only 20% of the Si nuclei of the starting hectorite form new phases while the rest stays forming part of the layered silicate, which demonstrates the high stability of this trioctahedral smectite in alkaline conditions.

Finally, the ^{29}Si MAS NMR spectrum of laponite after the hydrothermal treatment (Fig. 4c, bottom) shows well resolved xonotlite resonances as well as a main signal which must include the Si resonances of laponite and a resonance corresponding to the Si nuclei in antigorite (at −93.1 ppm in the pure mineral, Kosuge et al., 1995), in agreement with the XRD data. The fitting of the spectrum (Table 4) shows an increase in the percentage of partially condensed Si tetrahedra with an anionic basal O in the laponite structure which can be interpreted as due to a partial dissolution of the layers. The sum of the three resonances corresponding to Si in laponite is 80%, while 15% of the Si nuclei in the sample correspond to xonotlite and 5% to antigorite.

As in the case of the dioctahedral samples, the Si signals corresponding to the clay shifts, in all three smectites, towards higher frequency values after the treatment. A lower occupation of the octahedral sheet in this case must also be responsible case for such shifts (Sanz and Serratosa, 1984).

4. Discussion

The results of the present study have shown that when the studied phyllosilicates are submitted to hydrothermal conditions in a Ca-rich alkaline medium, the degree of transformation of the Si environments in dioctahedral clays is much higher than that observed in the trioctahedral members. Thus, in dioctahedral samples ca. 54–67% of the Si atoms abandon the clay to form new phases, while 22–59% of the Si atoms in the trioctahedral members form other phases. This fact is important in the application of clays as the sealing material in projected nuclear waste repositories and suggests that the use of some trioctahedral component in the clay barrier would contribute to an increase its stability. An additional advantage of using trioctahedral phyllosilicates as part of the clay buffer is that all of them produce, at least in the present conditions, xonotlite as a reaction product, a Ca silicate hydrate which has been assessed for immobilization of radioactive waste (McCulloch et al., 1985). The full occupation of the octahedral sheet in the starting material is, therefore, a decisive factor in the stability of the clays in alkaline conditions being even more important than the nature of the layer itself, i.e., number of sheets making up a layer (2:1 or 1:1) and expandability. Thus, the well-crystallised kaolinite (1:1 non-expandable phyllosilicate composed of Si and Al) shows the same degree of transformation as beidellite (2:1 expandable phyllosilicate with the same composition).

On the other hand, the poorly-crystallised kaolinite sample is more reactive than the well-crystallised kaolinite, as demonstrated by the% of Si environments transformed as a consequence of the hydrothermal reaction: 67% in the poorly-crystallised kaolinite versus 57% in the well-crystallised kaolinite. The lower crystallinity of the former is very likely the factor favouring the higher degree of transformation. The same is observed in the trioctahedral members, hectorite and laponite (a synthetic poorly crystallised hectorite): 22% of the Si atoms in laponite form new phases while only 20% do so in hectorite. The higher similarity in the behaviour of these two trioctahedral members versus both kaolinite samples reinforces the higher stability of trioctahedral samples versus dioctahedral ones in alkaline conditions. It has to be pointed out that laponite particles are much smaller than hectorite ones, so that this fact also contributes to the higher reactivity of the former.

Another interesting point is that saponite, a trioctahedral phyllosilicate, shows a much lower stability than the two other trioctahedral members; this fact can be explained on the basis of the presence of Al in the tetrahedral sheet of the clay. The deconvolution ^{29}Si MAS NMR spectrum of the treated saponite sample shows that the% of Q^3(1Al) and Q^3(2Al) environments in the remaining clay decreases with respect to the values found in the starting material, indicating that the tetrahedral Si atoms located close to the Al atoms are more reactive in forming new phases. This is reasonable given the higher Si–O bonding energy as compared to the Al–O one. A similar behaviour was observed during the hydrothermal reaction of a Lu-homoionised saponite to form $Lu_2Si_2O_7$ (Alba et al., 2001). Although beidellite also contains Al substituting for Si in the tetrahedral sheet, as saponite, the % of Q^3(1Al) and Q^3(2Al) environments in the remaining clay increase with respect to the starting material as a consequence of the Al diffusion from the octahedral sheet to the vacant tetrahedral positions created after the migration of the Si atoms to the new phases.

Finally, the formation of different $CaSi_2Al_2O_8$ polymorphs from the dioctahedral samples deserves an additional comment. $CaSi_2Al_2O_8$ has several reported polymorphic forms: triclinic, hexagonal and orthorhombic, the triclinic phase being the thermodynamically stable one at all temperatures (Davis and Tuttle, 1952; Hong et al., 1999). The XRD patterns show that all dioctahedral phyllosilicates produce $CaSi_2Al_2O_8$ as a consequence of hydrothermal treatment in $Ca(OH)_2$. However, while the hexagonal phase of $CaSi_2Al_2O_8$ is the main product of the treatment of beidellite and

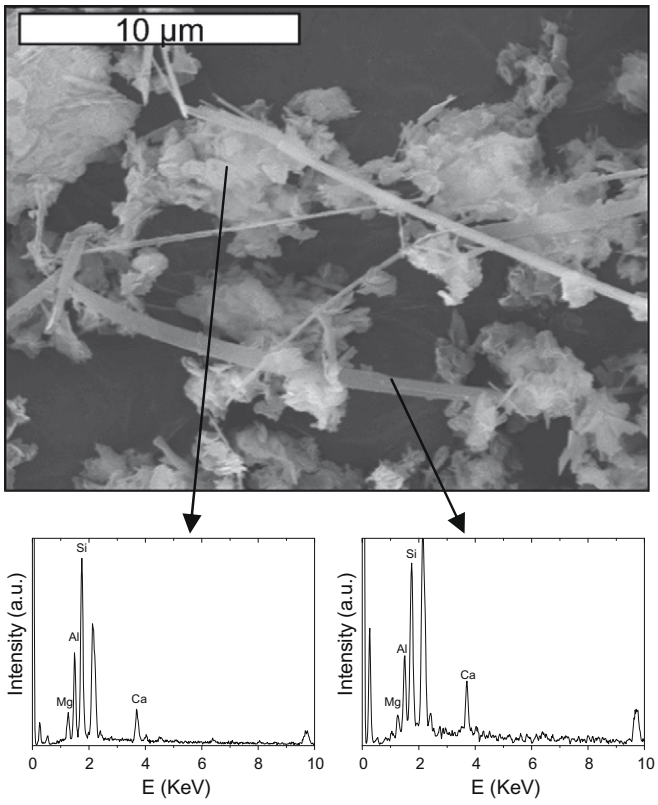

Fig. 6. SEM micrograph of the treated montmorillonite sample and EDX spectra associated with the particles marked with arrows.

both kaolinite samples, the treatment of montmorillonite produces anorthite (the triclinic form of $CaSi_2Al_2O_8$). Both montmorillonite and beidellite are 2:1 phyllosilicates while kaolinite is formed by 1:1 layers; therefore, the formation of one or another polymorph does not seem to be dependent on the nature of the silicate layer itself, i.e., it is not conditioned by the parent structure. The key could be in the chemical composition of the octahedral sheet; 68% of the occupied octahedral sites are filled with Al in the montmorillonite sample, the rest being mainly Mg and some Fe; in contrast, beidellite and both kaolinite samples contain Al in more than 90% of the occupied octahedral sites. This suggests that the presence of Mg could favour the formation of the low symmetry form if it enters the Ca sites. Considerable solid solution has been observed with $NaAlSi_3O_4$ but no studies of the solubility of Mg into $CaSi_2Al_2O_8$ have been reported to the authors' knowledge. The SEM/EDX analysis of the samples seems to support this hypothesis. Fig. 6 shows the micrograph of the treated montmorillonite sample where two different morphologies are observed: lamellar and fibrous particles; both of them show an associated EDX spectrum with Si, Al, Ca and Mg peaks, with the Mg contribution slightly more pronounced in the lamellar particles, which must correspond to the remaining montmorillonite, while the fibres must correspond to anorthite. Further studies on the local environment of Mg are necessary in order to confirm this hypothesis.

5. Conclusions

Trioctahedral phyllosilicates are much more stable than dioctahedral ones when submitted to hydrothermal treatment in a solution of $Ca(OH)_2$. The nature and expandability of the layer does not seem to influence the stability of the clay, so that a 2:1 expandable phyllosilicate, like beidellite, shows the same reactivity as the chemically analogous well-crystallised kaolinite sample, which is a 1:1 non-expandable phyllosilicate. However other factors like the poor crystallinity of the starting material or the presence of Al in the tetrahedral sheet of trioctahedral phyllosilicates weaken the clay structure in alkaline conditions and favour transformation towards other phases.

Acknowledgments

M.C. Jiménez is gratefully acknowledged for help with SEM/EDX. Financial support has been obtained from the following projects: Project funded within the VI Framework Programme as an HRM Activity under contract number MRTN-CT-2006-035957, DGICYT Project No. CTQ2007-63297 and an Excellence Project from Junta de Andalucía P06-FQM-02179.

References

Alba, M.D., Chain, P., 2007. Persistence of lutetium disilicate. Appl. Geochem. 22, 192–201.
Alba, M.D., Becerro, A.I., Castro, M.A., Perdigón, A.C., 2001. Hydrothermal reactivity of lu-saturated smectites: Part II. A short-range order study. Am. Miner. 86, 124–131.
Allen, C.C., Wood, M.I., 1988. Bentonite in nuclear waste disposal: a review of research in support of the basalt waste isolation project. Appl. Clay Sci. 3, 11–30.
Andersson, K., Allard, B., Bengtsson, M., Magnusson, B., 1989. Chemical composition of cement pore solutions. Cem. Concr. Res. 19, 327–332.
Becerro, A.I., 1997. Ph.D. Thesis, Univ. Seville.
Bauer, A., Berger, G., 1998. Kaolinite and smectite dissolucion rate in high molear KOH solutions at 35 °C and 80 °C. Appl. Geochem. 13, 905–916.
Bauer, A., Velde, B., Berger, G., 1998. Kaolinite transformation in high molar KOH solutions. Appl. Geochem. 13, 619–629.
Bentabol, M., Ruiz Cruz, M.D., Huertas, F.J., Linares, J., 2003. Hydrothermal transformation of kaolinite to illite at 200 °C and 300 °C. Clay Miner. 38, 161–172.
Carpentier, T., Ispas, S., Profeta, M., Mauri, F., 2004. First-principles calculation of ^{17}O, ^{29}Si and ^{23}Na NMR spectra of sodium silicate crystals and glasses. J. Phys. Chem. B 108, 4147–4161.
Chain, P., 2007. Ph.D. Thesis, Univ. Seville.
Cong, X., Kirkpatrick, R.J., 1996. Si-29 MAS NMR study of the structure of calcium silicate hydrate. Adv. Cem. Based Mater. 3, 144–156.
Davis, G.L., Tuttle, F., 1952. The new crystalline phases of the anorthite composition $CaO\ Al_2O_3\ 2SiO_2$. Am. J. Sci. Bowen 10, 7–114.
Desprairies, A., 1983. Relation entre le parametre b des smectites et leer contenu en fer et magnesium. Application a letude des sediments. Clay Miner. 18, 165–175.
Glasser, F.P., 2001. Mineralogical aspects of cement in radioactive waste disposal. Mineral. Mag. 65, 621–633.
Grim, R.E., 1968. Clay Mineralogy. McGraw-Hill Book Company, New York.
Hansen, M.R., Jakobsen, H.J., Skibsted, J., 2003. ^{29}Si chemical shift anisotropies in calcium silicates from high-field ^{29}Si MAS NMR spectroscopy. Inorg. Chem. 42, 2368–2377.
Hong, S.-H., Young, J.F., Yu, P., Kirkpatrick, R.J., 1999. ^{29}Si MAS NMR study of the structure of calcium silicate hydrate. Adv. Cem. Based Mater. 14, 1828–1833.
Huang, W.L., 1993. The formation of illitic clays from kaolinite in KOH solution from 225 °C to 350 °C. Clays Clay Miner. 41, 645–654.
Kirkpatrick, R.J., Kinsey, R.A., Smith, K.A., Henderson, D.M., Oldfield, E., 1985. High-resolution solid-state Na-23, Al-27, and Si-29 nuclear magnetic-resonance spectroscopic reconnaissance of alkali and plagioclase feldspars. Am. Miner. 70, 106.
Kosuge, K., Shimada, K., Tsunashima, A., 1995. Micropore formation by acid treatment of antigorite. Chem. Mater. 7, 2241–2246.
Liebau, F., 1985. Structural Chemistry of Silicates. Springer-Verlag, Berlin.
Massiot, D., Fayon, F., Capron, M., King, I., Le Calvé, S., Alonso, B., Durand, J.O., Bujoli, B., Gan, Z., Hoatson, G., 2002. Modelling one- and two-dimensional solid-state NMR spectra. Magn. Reson. Chem. 40, 70–78.
Mather, J.D., Chapman, N.A., Black, J.H., Lintern, B.C., 1982. The geological disposal of high-level radioactive waste – a review of the institute of geological sciences research programme. Nucl. Energy 21, 167–173.
McCulloch, C.E., Angus, M.J., Crawford, R.W., Rahman, A.A., Glasser, F.P., 1985. Mineral. Mag. 49, 211–218.
Noma, H., Adachi, Y., Matsuda, Y., Yokoyama, T., 1998. ^{29}Si and ^{1}H MAS NMR of natural and synthetic xonotlite. Chem. Lett. 3, 219–220.
Pusch, R., Yong, R., 2003. Water saturation and retention of hydrophilic clay buffer – microstructural aspects. Appl. Clay Sci. 23, 61–68.
Pusch, R., Zwahr, H., Gerber, R., Schomburg, J., 2003. Interaction of cement and smectite clay – theory and practice. Appl. Clay Sci. 23, 203–210.
Ramírez, S., Cuevas, J., Vigil, R., Leguey, S., 2002. Hydrothermal alteration of "La Serrata" bentonita (Almería, Spain) by alkaline solutions. Appl. Clay Sci. 21, 257–269.
Ramírez, S., Righi, D., Petit, S., 2005. Alteration of smectites induced by hydrolitic exchange. Clay Miner. 40, 15–24.
Rassineux, F., Griffault, L., Meunier, A., Berger, G., Petit, S., Viellard, P., Zellagui, R., Munoz, M., 2001. Expandibility-layer stacking relationship during experimental alteration of a Wyoming bentonite in pH 13.5 solutions at 35 °C and 60 °C. Clay Miner. 36, 197–210.
Read, D., Glasser, F.P., Ayora, C., Guardiola, M.T., Sneyers, A., 2001. Mineralogical and microstructural changes accompanying the interaction of boom clay with ordinary Portland cement. Adv. Cem. Res. 13, 175–183.
Reardon, E.J., 1990. An ion interaction model for the determination of chemical equilibrium in cement/water systems. Cem. Concr. Res. 20, 175–192.
Sánchez, L., Cuevas, J., Ramírez, S., Ruiz de León, D., Fernández, R., Vigil, R., Leguey, S., 2006. Geochemical reactions of FEBEX bentonite in hyperalkaline conditions resembling the cement–bentonite interface. Appl. Clay Sci. 33, 125–132.
Sanz, J., Serratosa, J.M., 1984. Si-29 and Al-27 high-resolution MAS-NMR spectra of phyllosilicates. J. Am. Chem. Soc. 106, 4790–4793.
Savage, D., Chapman, N.A., 1982. Hydrothermal behaviour of simulated waste glass – and waste–rock interaction under repository conditions. Chem. Geol. 36, 59–86.
Savage, D., Noy, D., Mihara, M., 2002. Modelling the interaction of bentonite with hyperalkaline fluids. Appl. Geochem. 17, 207–223.
Sheriff, B.L., Grundy, H.D., Hartman, J.S., Hawthorne, F.C., 1991. The incorporation of alkalis in beryl – multinuclear MAS NMR and crystal-structure study. Can. Miner. 29, 271–276.
Vieillard, P., Rassineux, F., 1992. Thermodynamic and geochemical modeling of the alteration of two cement matrices. Appl. Geochem. 1, 125–136.
Vigil, R., Cuevas, J., Ramírez, S., Leguey, S., 2001. Zeolite formation during the alkaline reaction of bentonite. Eur. J. Miner. 13, 635–644.
Wheeler, P.A., Wang, J.Z., Baker, J., Mathias, L.J., 2005. Synthesis and characterization of convalently functionalized laponite clay. Chem. Mater. 17, 3012–3018.
Woessner, D.E., 1989. Characterization of clay minerals by ^{27}Al nuclear magnetic resonance spectroscopy. Am. Miner. 74, 203–215.